Arch. Mech., **51**, 6, pp. 805–832, Warszawa, 1999

Transformation conditions in an Fe-based shape memory alloy: an experimental study

K. TANAKA and T. WATANABE

Department of Aerospace Engineering
Tokyo Metropolitan Institute of Technology
J-191-0065 Hino/Tokyo, Japan
e-mail: kikitana@astan1.tmit.ac.jp

MARTENSITE AND AUSTENITE START conditions are studied experimentally in an Fe–9% Cr–5%Ni–14%Mn–6%Si polycrystalline SMA under combined tension/compression-torsion loads. The martensite start condition is represented by an oval cone in the stress-temperature space, thus being different from the von Mises theory. The third invariant of the stress deviator has a marked effect. The austenite start condition is expressed by a polygonal cone in the same stress-temperature space. Each side of the cone corresponds to the martensite variants preferably induced during mechanical loading. The direction of the austenite start plane is determined by the direction of loading whereas the amount of variants governs the position of the plane.

Keywords: Martensite start surface, Austenite start plane, Fe-based shape memory alloy, Torsion-tension (compression) tests, Stress-temperature space, Transformation conditions, non-proportional loading

1. Introduction

WHEN DESIGNING EFFECTIVE shape memory devices, one needs possibly abundant knowledge of the thermomechanical performance of the shape memory alloys (SMAs) used in the devices, under such complex situations as the cyclic thermomechanical loading, the high frequency input or the multiaxial stress states. For example, SMA composites, a sort of intelligent (smart) structures composed of a SMA component and a matrix material, should be designed by taking precisely into account of the SMA response under multiaxial stresses, although the composities themselves are subjected to a simple load [1 – 3].

Only a few papers have, however, been published on the experiments of SMAs under multiaxial stress states; SITTNER and TOKUDA [4 – 6] and ROGUEDA *et al.* [7] in Cu-based SMA, NISHIMURA *et al.* [8 – 9] in Fe-based SMA and RANIECKI *et al.* [10] in TiNi SMA. Difficulties consist in the fact that the highly computerized experimental system is required for supplying sound data. The preparation for a

large test specimen, usually a thin-walled tubular specimen, which fits the tests under multiaxial stresses and exhibits a stable response under repeated loading, is rather a difficult problem to be solved before starting the experiments [11]. The flow rule for the transformation strain and the associated normality law, the transformation start/finish conditions, the stress-strain-temperature hystereses were some of the themes investigated. Asymetry of the martensite start surface in the stress-temperature space was clearly observed in all SMA systems, thus approving the theory with the third invariant of stress tensor [10, 12], which has been suggested in the micromechanical study by PATOOR *et al.* [13, 14]. The accumulation of sound data is still urgently necessary to establish a rational theoretical framework on thermomechanical behavior of SMAs.

In this paper, following the study of the transformation conditions in an Fe-9%Cr-5%Ni-14%Mn-6%Si polycrystalline SMA by the same authors [8, 9, 15 – 20], the martensite and austenite start conditions are investigated from the experimental point of view under the combined tension/compression-torsion loads. The asymmetry of the martensite start surface in the stress-temperature space is shown to be explained by the theory proposed by RANIECKI *et al.* [10, 12]. The austenite start condition is revealed to be represented by a polygonal cone in the same stress-temperature space, the shape and position of which depend on the amount of the martensite phase and the type of martensite variants preferably induced during mechanical loading.

2. Alloy and experimental procedures

An Fe-9%Cr-5%Ni-14%Mn-6%Si polycrystalline SMA, which is the same material as that studied in the previous papers by the same authors [8, 9, 15 – 20], was tested. Its chemical composition and mechanical properties at room temperature (RT, 303 K) are tabulated in Tables 1 and 2, respectively. The thin-walled tubular specimen employed in the tests, 6 mm in outer diameter, 4 mm in inner diameter and 20 mm in gauge length, is sketched in Fig. 1.

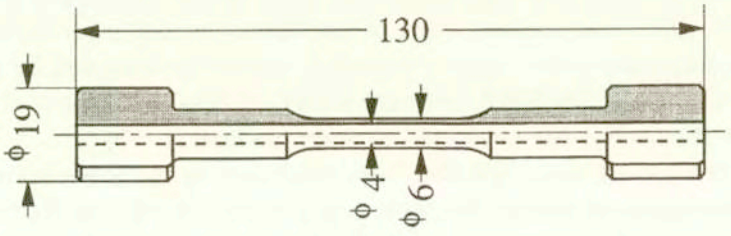

FIG. 1. Test specimen.

Table 1. Alloy composition (wt.%).

Cr	Ni	Mn	Si	C	N	Fe
9.0	5.2	14.4	6.0	0.02	0.005	Bal.

Table 2. Mechanical properties at room temperature.

0.2% proof stress	Tensile strength	Elongation	Area contraction	Elastic constants	
$\sigma_{0.2}$ MPa	σ_f MPa	ϕ %	ψ %	E GPa	G GPa
258	788	70.5	61.1	172	62

In order to obtain better shape memory performance, the following training is carried out four times successively [15, 19]: The specimen was first mechanically loaded in tension to 4% at RT, and then unloaded to the stress-free state. A thermal heating up to 873 K, holding there for 600 s and succesive cooling to RT then followed. To guarantee a stable thermomechanical response, the specimens were further subjected, prior, to the test to an additional 30 cycles of thermomechanical training: a cycle of the training is composed of an isothermal loading/unloading to 350 MPa at RT and the subsequent stress-free heating/cooling to complete the reverse transformation.

Tests were carried out by means of a servo-hydraulic testing machine (SHIMADZU, EHF–ED5/TD05–10L) equipped with a high-frequency induction heater. The tensile displacement and the angle of twist between the gauge marks were measured independently by the eddy-current sensors, while the temperature of the specimen was detected by a platinum platinum-rhodium thermocouple spot-welded at the center of the gauge length. All experimental procedures were monitored and controlled by a personal computer. The output data of the tests were stored in the PC memory for later analyses. The axial stress σ and the shear stress τ were applied simultaneously to the specimen by means of the axial force and the torque. The proportional loading path $\tau = m\sigma$ on $\sigma - \tau$ plane is identified by the path parameter m.

The stress and strain intensities are introduced to measure the progress of deformation;

$$\sigma^{\text{int}} = \sqrt{\sigma^2 + (\sqrt{3}\tau)^2}, \qquad \varepsilon^{\text{int}} = \sqrt{\varepsilon^2 + (\gamma/\sqrt{3})^2}, \tag{2.1}$$

where ε and γ stand for the axial and shear strain, respectively. Henceforth, the shear stress τ^* and the shear strain γ^* defined by

$$\tau^* = \sqrt{3}\tau, \qquad \gamma^* = 1/\sqrt{3}\gamma, \tag{2.2}$$

are often used for simplicity. The proportional loading path may be represented also by $\tau^* = m^*\sigma$ on the $\sigma - \tau^*$ plane, when a new path parameter m^* is given by $m^* = \sqrt{3}m$.

The axial transformation strain ε_{T} and the shear transformation strain γ_{T} are evaluated by the formulae

$$\varepsilon_{\mathrm{T}} = \varepsilon - \frac{\sigma}{E}, \qquad \gamma_{\mathrm{T}} = \gamma - \frac{\tau}{2G}, \tag{2.3}$$

where the Young's modulus E and the shear modulus G were determined by the experimental data, test by test. In this sense, their temperature-dependence is taken into account. The transformation strain intensity was calculated from

$$\varepsilon_{\mathrm{T}}^{\mathrm{int}} = \sqrt{\varepsilon_{\mathrm{T}}^2 + (\gamma_{\mathrm{T}}^*)^2}, \qquad \gamma_\tau^* = \gamma_{\mathrm{T}}/\sqrt{3}. \tag{2.4}$$

The specimen was loaded isothermally at RT along the proportional loading path m, over the martensite start stress σ_{Ms}^m (RT), up to the maximum stress

$$\sigma_{\max}^{\mathrm{int}} = \sqrt{(\sigma_{\max})^2 + (\tau_{\max}^*)^2}, \qquad \tau_{\max}^* = \sqrt{3}\tau_{\max}. \tag{2.5}$$

The martensite variants are induced during the loading from σ_{Ms}^m (RT) to $\sigma_{\max}^{\mathrm{int}}$.

The martensite variants formed during pre-stressing transform back to the parent phase in the subsequent heating process under constant hold stresses (σ_h, τ_h) or (σ_h, τ_h^*); $\tau_h^* = \sqrt{3}\tau_h$. The austenite start temperatures T_{As} can be determined by monitoring the $\varepsilon_T - T$, $\gamma_T - T$ or $\varepsilon_T^{\mathrm{int}} - T$ dilatation curve during heating if the transformation is assumed to start when the transformation strain ε_T, γ_T or $\varepsilon_T^{\mathrm{int}}$ reaches an offset 0.05%. For a sufficient number of tests with different values of (σ_h, τ_h^*), one can construct an austenite start surface in the axial hold stress (σ_h)-shear hold stress (τ_h^*)-temperature (T) space, the form and location of which depends strongly on the direction and amount of pre-stressing, as will be clear in the following discussion.

3. Martensite start surface under proportional loading

The martensite start stress $\sigma_{\mathrm{Ms}}^m(T_h)$ during proportional loading m (or $m^* = \sqrt{3}m$), defined of 0.05% -proof-stress, are plotted in Fig. 2 at three different test temperatures $T_h = 303$, 323 and 343 K. The result clearly shows asymmetry of the martensite start curves with respect to the shear stress axis, meaning that the compressive stress retards the martensitic transformation. The phenomenon, observed also in other SMA systems [21, 22], is investigated from the continuum-mechanical point of view by RANIECKI *et al.* [10, 12] and from the micromechanical point of view by PATOOR *et al.* [13, 14], by introducing the third invariant of the stress deviator.

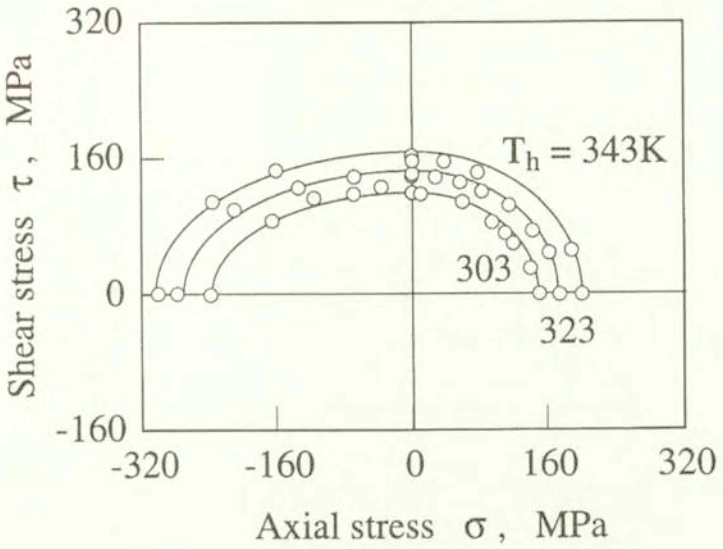

FIG. 2. Martensite start stresses during proportional loading; martensite start curves.

WERT *et al.* have clearly shown in their simulations based on metallurgy of SMAs that the martensite start condition of the stress-induced martensitic transformation is represented by a irregular polygon on the stress plane [23, 24]. Each side of the polygon corresponds to the martensite start conditions of the martensite variants which are preferably developed during loading. The martensite start curve determined in Fig. 2 is nothing else than a curve inscribed in such a polygon.

RANIECKI *et al.* [10, 12] proposed the following condition, representing the martensite start curve:

$$\sigma^{\mathrm{T}} = \frac{\sqrt{3}k(T)}{f(y,T)}, \qquad F = \sigma_{\mathrm{ef}} - \sigma^{\mathrm{T}}(y,t) = 0, \tag{3.1}$$

where another path parameter y is defined by

$$y \equiv 3\sqrt{6}\frac{J_3}{(J_2')^{3/2}};$$
$$J_2' \equiv \frac{2}{3}\sigma_{\mathrm{ef}}^2 = S_{ij}S_{ij}, \qquad J_3' \equiv \det S_{ij} = \frac{1}{3}\mathrm{tr}(\mathbf{S})^3, \tag{3.2}$$

with the second and third invariants J_2' and J_3' of the stress deviator $\mathbf{S}$. The temperature-dependent function $k(T)$ stands for the critical shear stress to start the martensitic transformation.

Note that $y = 0$ means the simple shear, whereas $y = +1$ and -1 stand for the simple tension and simple compression, respectively, and that $-1 \leq y \leq 1$.

The shape function $f(y,T)$ in Eq. (3.1), when normalized so that $f(0,T) = 1$, has the form

$$f(y,T) = \frac{\sigma^{\mathrm{T}}(0,T)}{\sigma^{\mathrm{T}}(y,T)}. \tag{3.3}$$

It should be emphasized that the condition (3.1) is reduced to the J_2-theory (von Mises theory) if $f = 1$.

When the data in Fig. 2 are evaluated by means of Eqs. (3.1) – (3.3), the values of the shape function are plotted in Fig. 3. The path-dependence of the shape function is clear, meaning that the J_3-theory proposed by RANIECKI *et al.* reasonably explains the present data. Contrary to their data in a TiNi SMA [10], the temperature-dependence is not observed in the present Fe-based SMA, at least at the temperature range investigated.

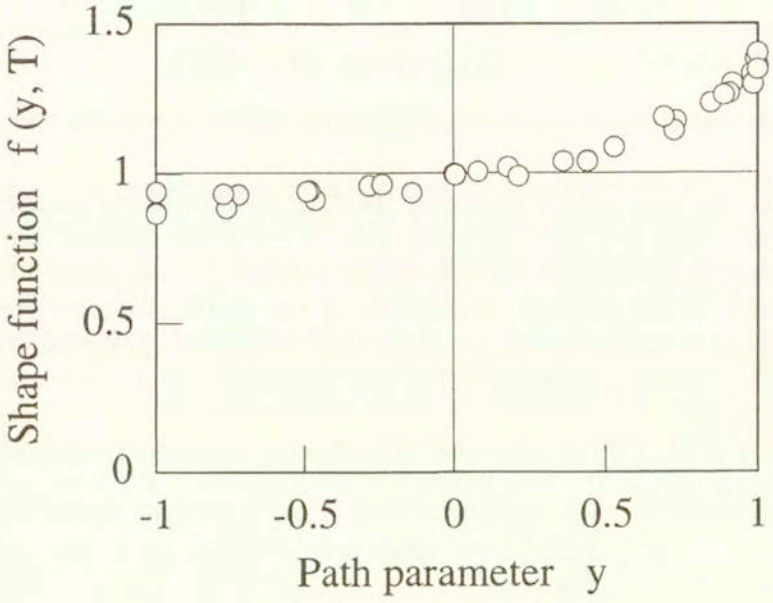

FIG. 3. Path- and temperature-dependence of shape function.

The martensite start condition of the present alloy is represented in the stress-temperature space as an oval cone illustrated schematically in Fig. 4. This surface corresponds to the initial yield surface in plasticity. When the reverse transformation progresses in the subsequent thermomechanical "unloading", the martensite start condition during thermomechanical "reloading" becomes quite different from the initial martensite start condition, as has been observed in the same Fe-based SMA by NISHIMURA *et al.* [16, 17] in the case of uniaxial loading. Generally the transformation condition depends strongly on the prior history of transformations in all SMA systems, resulting in complex stress-strain-temperature hystereses in

thermomechanical loading. The "subsequent" martensite start condition during thermomechanical loading should be an urgent theme to be investigated whether or not the condition might be a potential such as the yield condition plays the role of the plastic potential in plasticity [25].

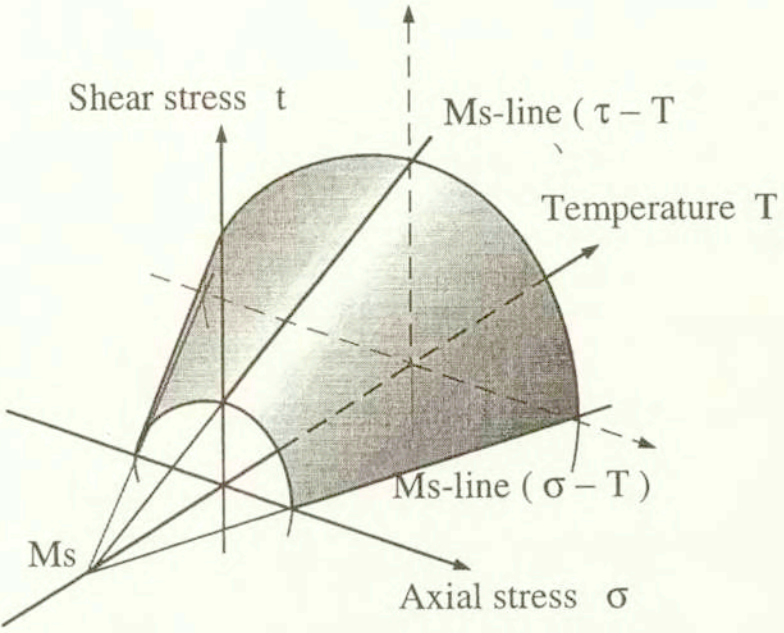

FIG. 4. Martensite start cone in stress-temperature space (Schematic).

One comment more on the martensite start cone in Fig. 4: during isothermal mechanical loading at lower temperature range, the reorientation of the temperature-induced martensite variants often progresses at low stress level [26 – 28]. The critical stress for the reorientation process is observed to be insensitive to the temperature, meaning that the condition can be represented by a cylindrical surface in the same stress-temperature space. The martensite start cone must be connected with this reorientation start cylinder at the lower temperature range. The uniaxial figure of such transformation/reorientation start condition was widely employed in the simulations of thermomechanical behavior in SMAs [29 – 33]. In the uniaxial case, the transformation/reorientation condition was shown to change its form and position on the stress-temperature plane during cyclic thermomechanical loading [34, 35]. The phenomenon should be investigated in the stress-temperature space in order to supply sound data for constructing a rational theoretical framework for transformation thermomechanics, in which the subsequent transformation condition must play a key role as a potential.

4. Austenite start plane

4.1. Austenite start line

Before going further, experimental results of uniaxial alloy response in the process of reverse transformation are summarized briefly [18]. The specimens were pre-stressed axially up to a maximum tensile stress $\sigma^{+0}_{\max}$ at RT. Here and henceforth, the superscript $+0$ means the pre-stressing along the path $m = +0$ (pure tension). The martensitic transformation starts at the martensite start stress $\sigma^{+0}_{Ms}(\mathrm{RT}) = 151$ MPa, and the amount of martensite variants M^{+0} increases in the subsequent loading process up to $\sigma^{+0}_{\max}$. Figure 5 plots the austenite start temperature $T^{+0/\varepsilon}_{As}$ versus the axial hold stress σ_h, showing clearly the linear austenite start lines, the $\mathrm{As}^{+0/\varepsilon}$-lines, with a slope $c^{+0/\sigma}_A = 2.1$ MPa/K. The lines correspond to the Clausius-Clapeyron relation. The superscript $+0/\varepsilon$ means that the austenite start temperature after pre-stressing along the path $m = +0$ is measured from $\varepsilon_T - T$ dilatation curves, whereas $+0/\sigma$ on c_A means that the data after pre-stressing along the path $m = +0$ are plotted on the $\sigma_h - T$ plane.

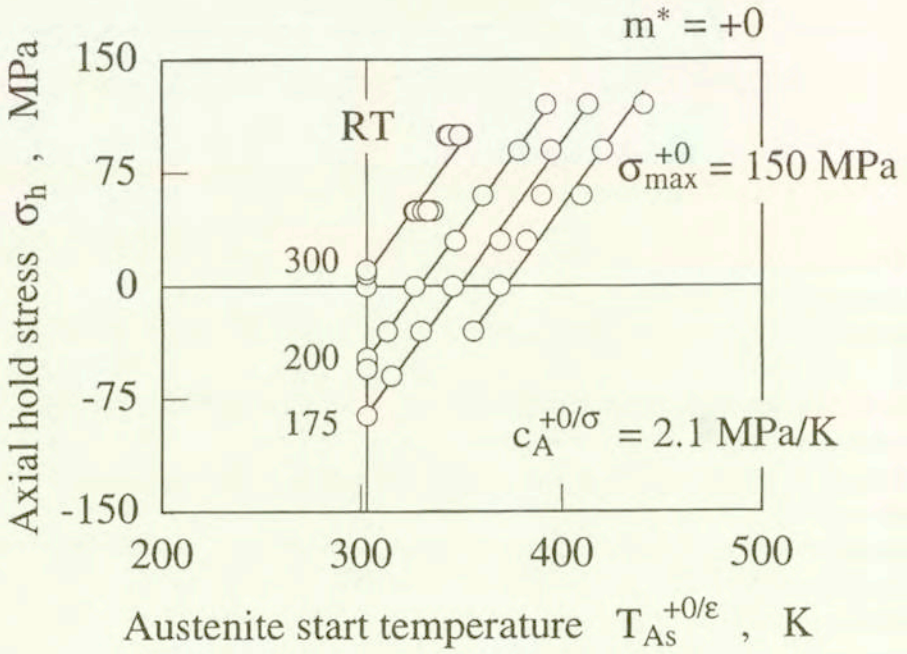

FIG. 5. Austenite start lines after tensile pre-stressing.

A different set of austenite start lines, the $\mathrm{As}^{-0/\varepsilon}$-lines, is observed as shown in Fig. 6 when the specimen is pre-stressed down to the maximum compressive stress

$\sigma_{\max}^{-0}$ at RT. The slope of the lines is $c_A^{-0/\sigma} = -2.4$ MPa/K. The transformation starts in this case at the martensite start stress $\sigma_{Ms}^{-0}(\mathrm{RT}) = -228$ MPa, and the martensite variants M^{-0} are formed from then on in the compressive loading process.

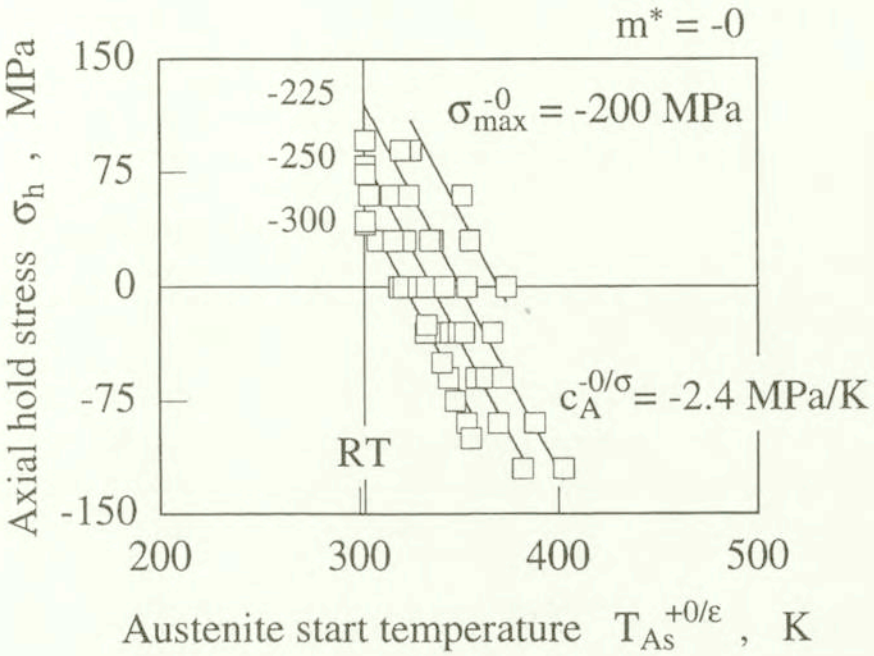

FIG. 6. Austenite start lines after compressive pre-stressing.

The following two characteristics of the austenite start lines should specially be emphasized in Figs. 5 and 6 in relation to the later discussion: Each set of austenite start lines corresponds to the martensite variants formed during prestressing. Directly speaking, the slope of the austenite start line depends on the direction of pre-stressing. Secondly, the austenite start lines translates to the lower temperature side without changing its slope when the maximum stress is larger; in other words, when the amount of martensite induced during loading is larger.

4.2. Austenite start plane after axial pre-stressing ($m = +0$)

The specimen was pre-stressed in tension up to $\sigma_{\max}^{+0} = 200$ MPa to produce the martensite variants M^{+0}. The austenite start temperatures $T_{\mathrm{As}}^{+0/\varepsilon}$ measured from $\varepsilon_T - T$ dilatation curves under hold stresses (σ_h, τ_h^*) are plotted in Fig. 7 with the shear hold stress as a parameter. The same data are re-plotted in Fig. 8

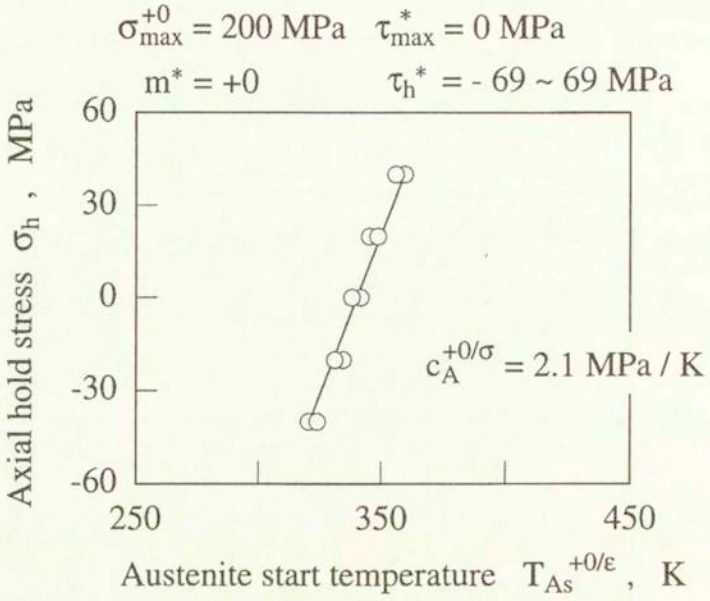

FIG. 7. Effect of axial hold stress on austenite start temperature: case of tensile pre--stressing.

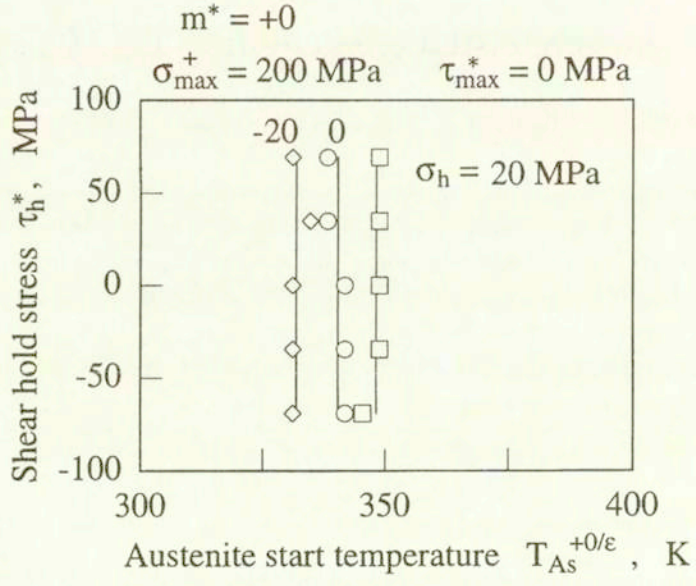

FIG. 8. Effect of shear hold stress on austenite start temperature: case of tensile pre--stressing.

with the axial hold stress as a parameter. Figures rationally conclude that the austenite start condition is represented by a plane in the axial hold stress (σ_h)-shear hold stress (τ_h^*) -temperature (T) space, as shown in Fig. 9. The austenite start plane, the $As^{+0/\varepsilon}$-plane, is perpendicular to the σ_h-T coordinate plane, and the thick solid line corresponds to the $As^{+0/\varepsilon}$ -line in Fig. 5 in the uniaxial case.

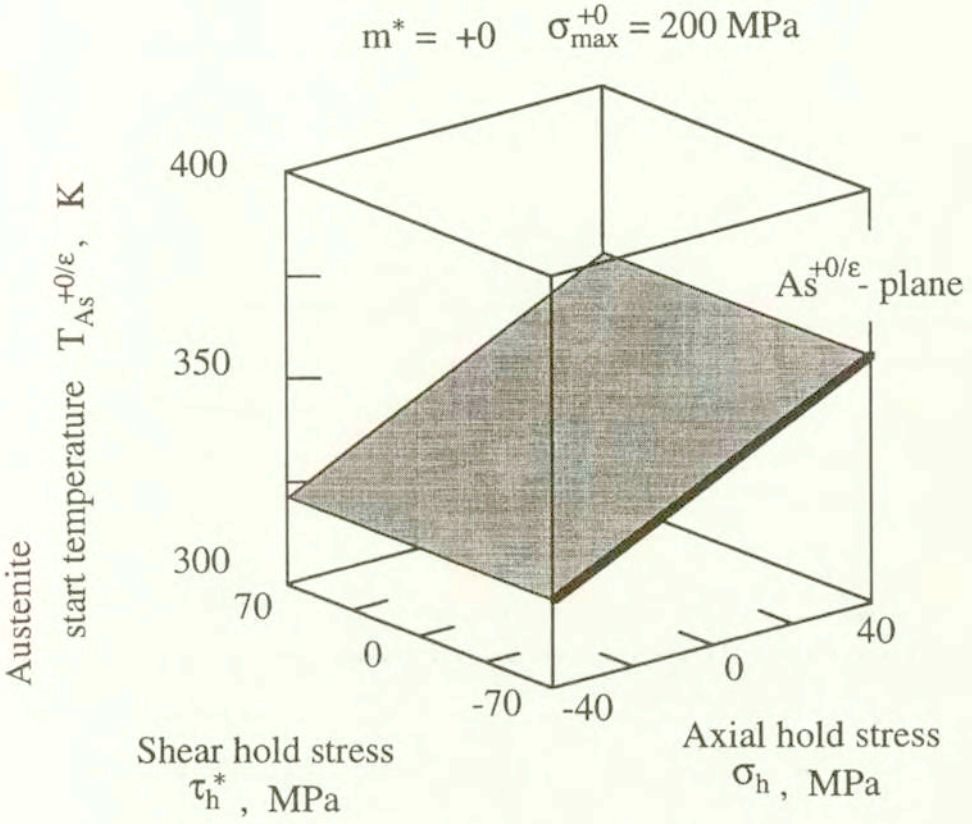

FIG. 9. Austenite start plane after tensile pre-stressing.

It is worth noting again that the $As^{+0/\varepsilon}$-plane in Fig. 9 denotes the condition to start the reverse transformation of the martensite variants M^{+0} which are induced during pre-stressing in tension.

4.3. Autensite start plane after shear pre-stressing ($m = \infty$)

The specimen was pre-stressed in torsion up to $\tau^*_{\max} = 284$ MPa ($\tau_{\max} = 164$ MPa), over the martensite start stress $\tau^*_{Ms}(\mathrm{RT}) = 217$ MPa ($\tau_{Ms} = 125$ MPa), to produce the martensite variants M^{∞} which are favorable to torsion. The austenite start temperatures $T_{\mathrm{As}}^{\infty/\gamma^*}$ measured from $\gamma^*_T - T$ dilatation curves

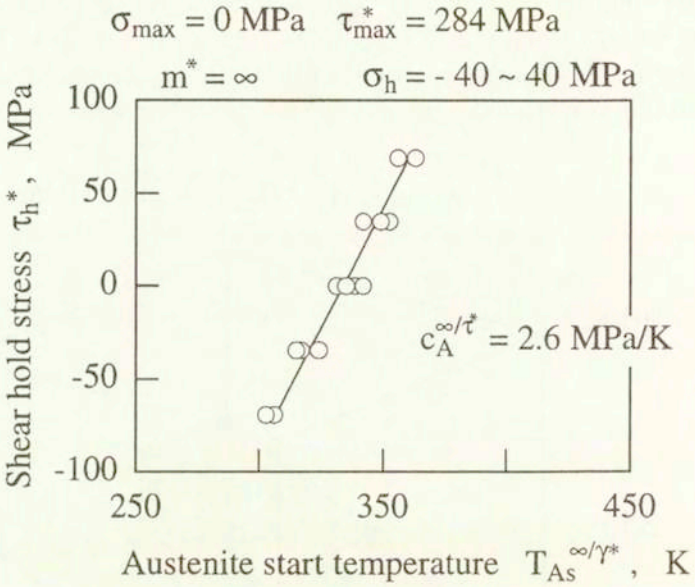

FIG. 10. Effect of shear hold stress on austenite start temperature: case of shear pre--stressing.

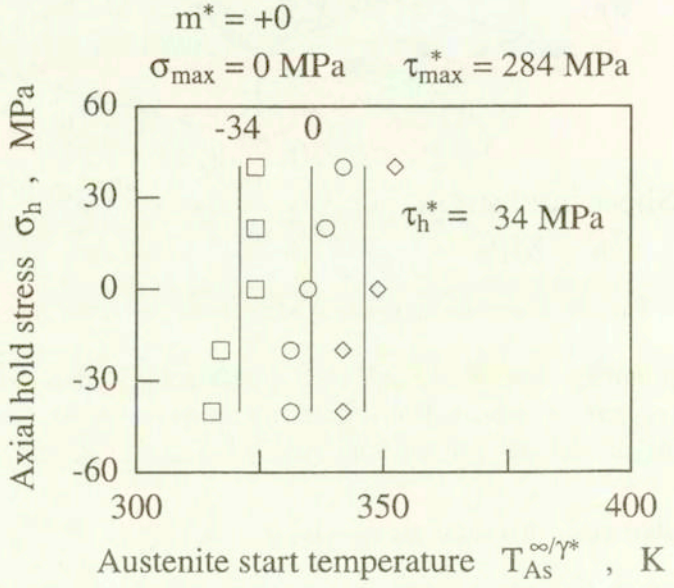

FIG. 11. Effect of axial hold stress on austenite start temperature: case of shear pre--stressing.

are plotted in Figs. 10 and 11, revealing again that the austenite start condition is represented by a plane, the $As^{\infty/\gamma*}$-plane, perpendicular to the $\tau_h^* - T$ coordinate plane (cf. Fig. 12). The intersection of the plane with the $\tau_h^* - T$ coordinate plane, denoted by the thick solid line in the figure, is nothing else than the austenite start line, the $As^{\infty/\gamma*}$-line with the slope $c_A^{\infty/\tau*} = 2.6$ MPa/K.

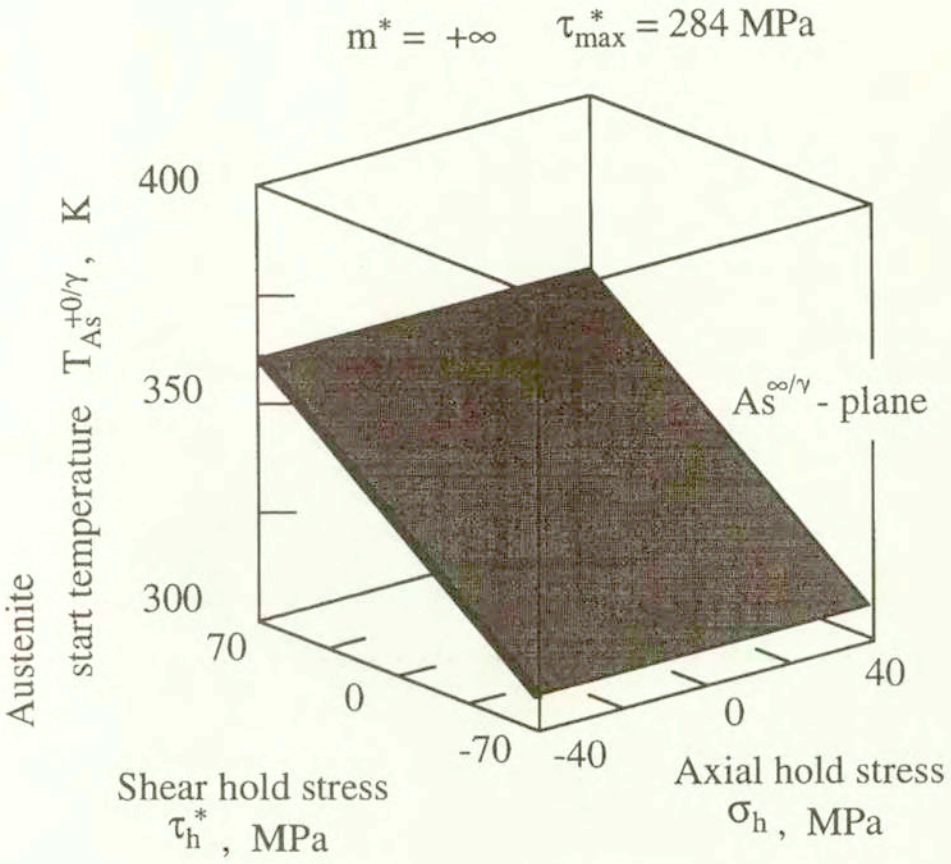

FIG. 12. Austenite start plane after shear pre-stressing.

4.4 Austenite start plane after proportional pre-stressing

Thermodynamics of martensitic transformation clearly explains the existence of not only the $As^{+0/\varepsilon}$- and $As^{\infty/\gamma*}$ -planes in Figs. 9 and 12 but also the As^{m^*}-planes which are observed after proportional pre-stressing along the path $m^*(-\infty < m^* < -0$ or $+0 < m^* < \infty)$ [8]. The following points have been proved by the present authors: When only one set of martensite variants, M^{m^*}, say, is formed during the loading along the path m^*, the iso-$T_{As}^{m^*}$ lines on the As^{m^*}-plane are, when they are projected onto the $\sigma_h - \tau_h^*$ -plane, prependicular

to the direction of pre-stressing $\tau^* = m^*\sigma$. Or equivalently, the austenite start temperature depends solely on the length of the projection of the hold stress vector (σ_h, τ_h^*) onto the direction of pre-stressing $(1, m^*)$;

$$\sigma_h^{\text{eff}} = \frac{\sigma_h + m^*\tau_h^*}{\sqrt{1+(m^*)^2}}, \tag{4.1}$$

which may be called the effective hold stress.

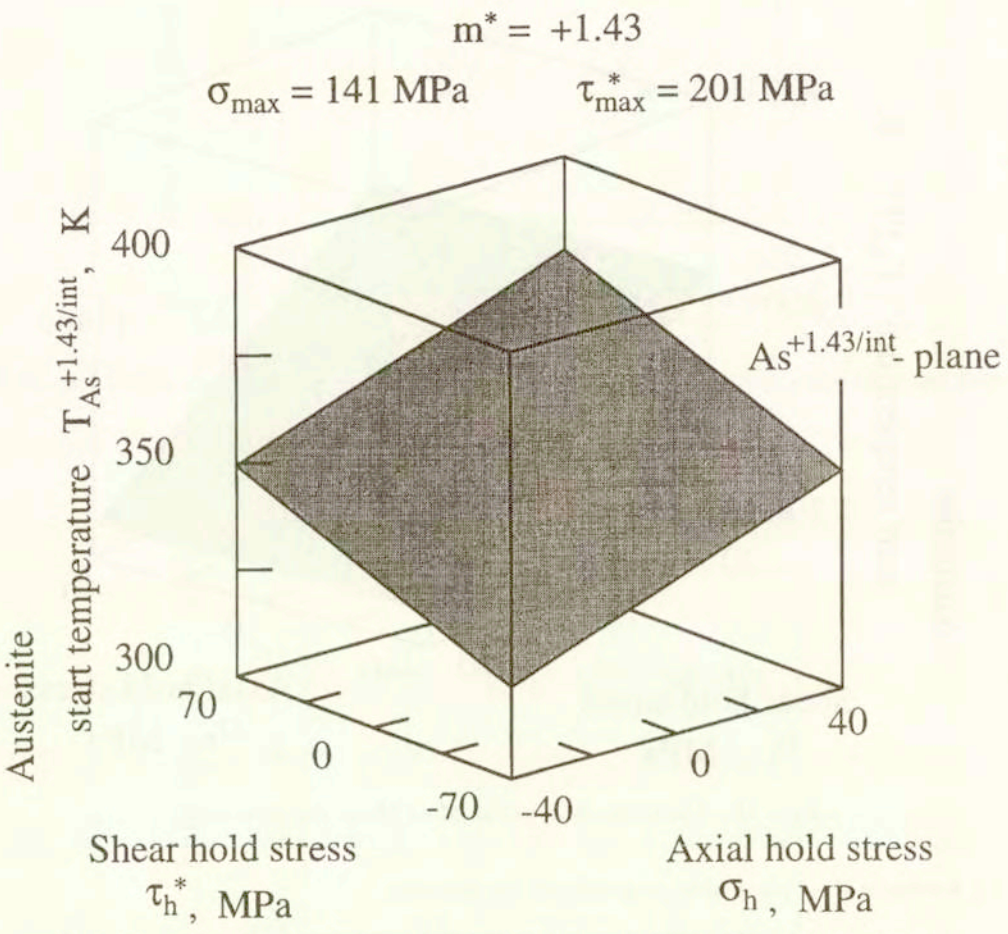

FIG. 13. Austenite start plane after proportional pre-stressing $m^* = +0.82$.

This theoretical prediction fully explains the experimental results after axial pre-stressing ($m^* = +0$) in Fig. 9 ($\sigma_h^{\text{eff}} = \sigma_h$ in this case), shear pre-stressing ($m^* = \infty$) in Fig. 12 ($\sigma_h^{\text{eff}} = \tau_h^*$ in this case), and the proportional pre-stressing along the path m^*; the case of $m^* = +1.43$ ($m = +0.83$) is given in Fig. 13. It should be noted that the austenite start temperatures necessary to construct

the plane in Fig. 13 were determined from the dilatation curves $\varepsilon_T^{\text{int}}$-T. Hence the superscript +1.43/int is used. The iso-$T_{\text{As}}^{+1.43/\text{int}}$ lines on the $\text{As}^{+1.43/\text{int}}$ -plane almost satisfy the geometrical configuration explained above. Figure 14, which contains all the data points forming the $\text{As}^{+1.43/\text{int}}$-plane in Fig. 13, well proves that the effective hold stress defined in Eq. (4.1) is an appropriate measure to determine the austenite start temperature. The slope of the line is $c_A^{+1.43/\text{eff}} = 2.1$ MPa/K.

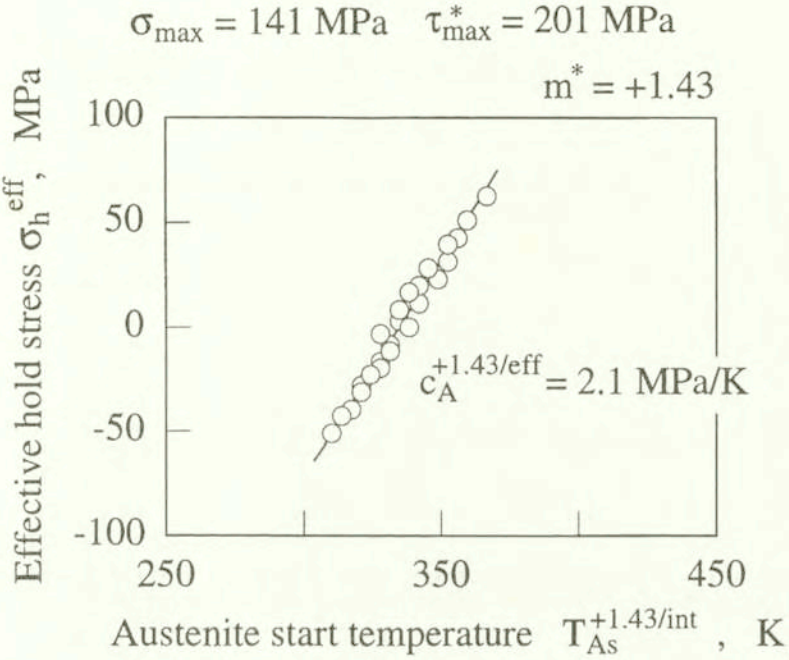

FIG. 14. Austenite start plane depending on effective hold stress: case of proportional pre-stressing $m^* = +0.82$.

4.5. Austenite start multi-planes after non-proportional pre-stressing: Shear pre-stressing followed by axial pre-stressing ($m^* = \infty \to +0$)

The austenite start plane after non-proportional pre-stressing is investigated in this subsection to show that the austenite start multi-planes are formed corresponding to martensite variants with some different orientations which are induced during pre-stressing.

The specimen was, in the first run, subjected to shear pre-stressing up to $\tau_{\text{max}}^* = 284$ MPa ($\tau_{\text{max}} = 164$ MPa) and unloaded. Tensile loading up to $\sigma_{\text{max}}^{+0} = 250$ MPa and unloading the follow in the second run. The austenite start temperatures were measured in the subsequent heating process under hold stresses (σ_h, τ_h^*).

Note that the maximum stresses $\tau^*_{\max}$ and $\sigma^{+0}_{\max}$ are higher than the martensite start stresses $\tau^*_{Ms}(\mathrm{RT}) = 217$ MPa and $\sigma^{+0}_{Ms}(\mathrm{RT}) = 151$ MPa, respectively. Therefore, the martensite variants M^{∞} which are favorable to the shear stress are induced during the first shear pre-stressing, whereas the martensite variants M^{+0} favorable to the tensile stress are expected to form during the subsequent axial pre-stressing. These two different types of variants are supposed to transform independently back in the subsequent heating process. Following the observation in Fe-based SMAs, the reorientation process $M^{\infty} \rightarrow M^{+0}$ is understood here not to progress in the second mechanical run [36].

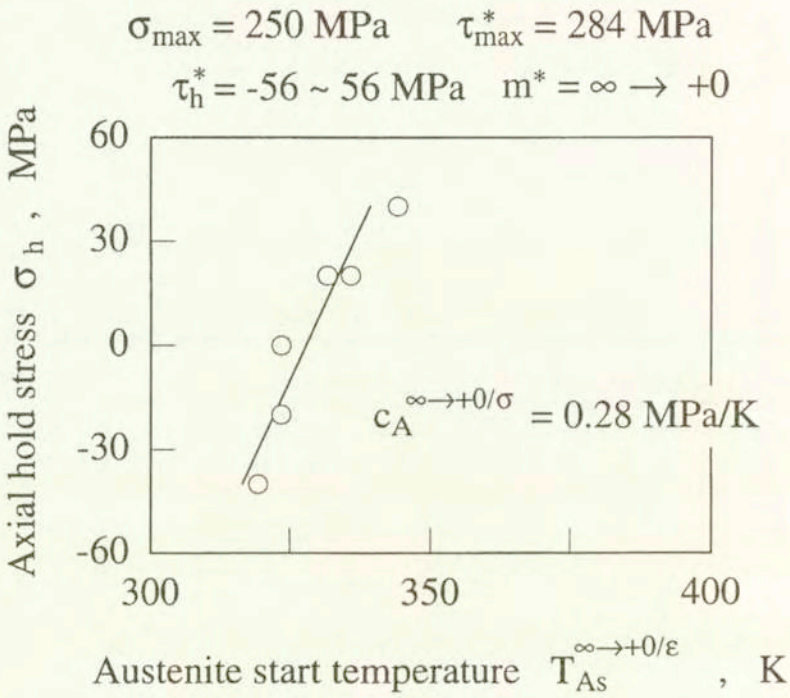

FIG. 15. Effect of axial hold stress on austenite start temperature after succesive pre-stressing $m^* = \infty$ and $m^* = +0$.

Figures 15 and 16 illustrate the austenite start temperature $T^{\infty\rightarrow+0/\varepsilon}_{\mathrm{As}}$ versus hold stresses, where the superscript $\infty \rightarrow +0/\varepsilon$ on T_{As} means that the austenite start temperatures after a successive pre-stressing $m = \infty$ and $m = +0$ are measured from $\varepsilon_T - T$ dilatation curves. The results again show that the austenite start condition is represented by a plane, the $\mathrm{As}^{\infty\rightarrow+0/\varepsilon}$ -plane, perpendicular to the $\sigma_h - T$ coordinate plane. Similar data were obtained for the austenite start temperatures $T^{\infty\rightarrow+0/\gamma^*}_{\mathrm{As}}$ measured from $\gamma^*_T - T$ dilatation curves (Figs. 17 and 18), showing that the austenite start plane, the $\mathrm{As}^{\infty\rightarrow+0/\gamma^*}$ -plane, is perpendicular to the $\tau^*_h - T$ coordinate plane.

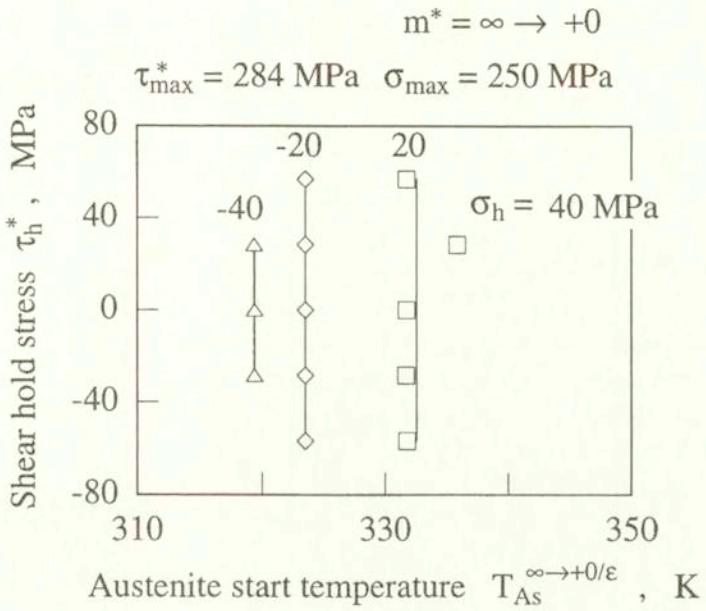

FIG. 16. Effect of shear hold stress on austenite start temperature after succesive pre--stressing $m^* = \infty$ and $m^* = +0$.

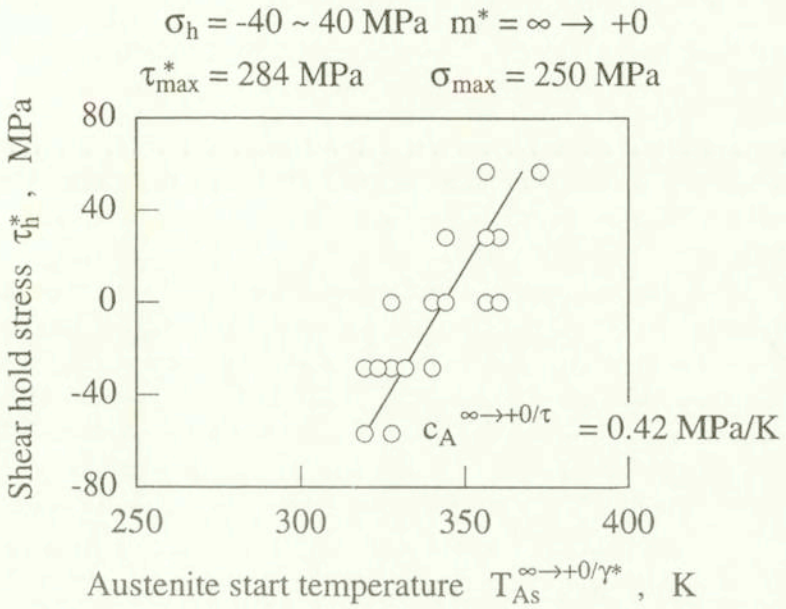

FIG. 17. Effect of shear hold stress on austenite start temperature after succesive pre--stressing $m^* = \infty$ and $m^* = +0$.

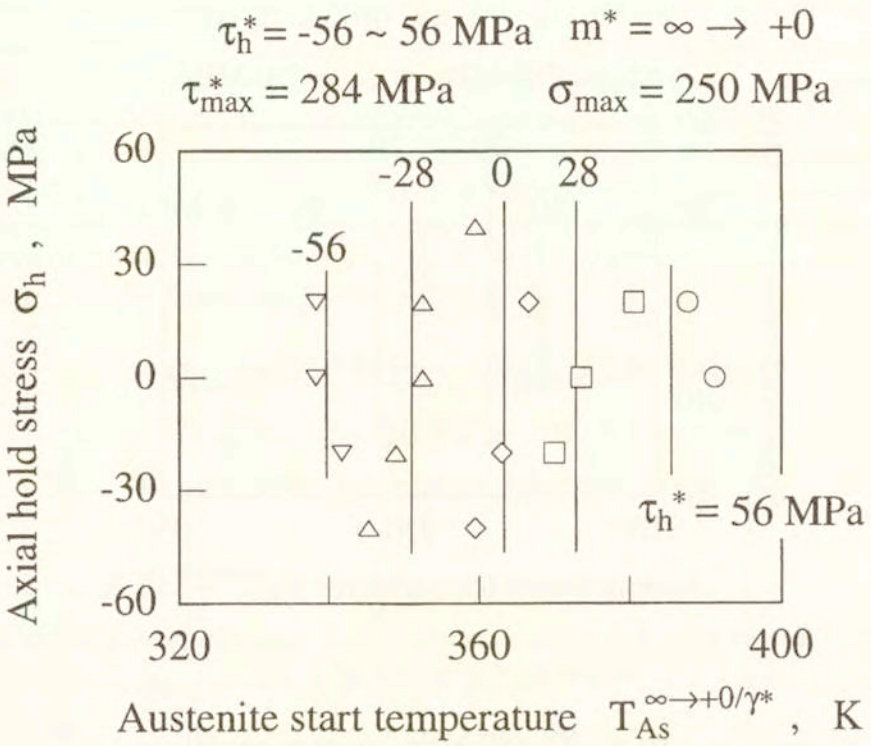

FIG. 18. Effect of axial hold stress on austenite start temperature after succesive pre--stressing $m^* = \infty$ and $m^* = +0$.

The two austenite start planes are drawn together in Fig. 19, which clearly reveals that, under all values of hold stresses tested here, the martensite variants M^{+0} transform back to the parent phase at lower temperature range than the M^{∞} variants do.

In Fig. 5 the following conclusion was drawn: the $As^{+0/\varepsilon}$ -line translates to the lower temperature side without changing its slope, when σ_{max}^{+0} is larger. In order to show that the same is true even in the multiaxial stress state, the specimen was subjected to shear prestressing up to $\tau_{max}^* = 329$ MPa ($\tau_{max} = 190$ MPa) follwed by a subsequent axial pre-stressing up to $\sigma_{max} = 250$ MPa. Note that the maximum shear stress is now larger than in the tests in Fig. 19, whereas the maximum tensile stress is the same in both tests. As before, the austenite start temperatures, $T_{As}^{\infty \rightarrow +0/\varepsilon}$ and $T_{As}^{\infty \rightarrow +0/\gamma^*}$, were measured independently from $\varepsilon_T - T$ and $\gamma_T^* - T$ dilatation curves, respectively. Under the condition $(\sigma_h, \tau_h^*) = (-20$ MPa, $5T$ MPa), the transformation strains ε_T and γ_T develop during heating as shown in Fig. 20. The axial transformation strain starts recovering as soon as the temperature starts to increase, whereas the shear transformation strain stays almost constant till it starts decreasing at a much ligher temperature $T_{As}^{\infty \rightarrow +0/\gamma^*}$.

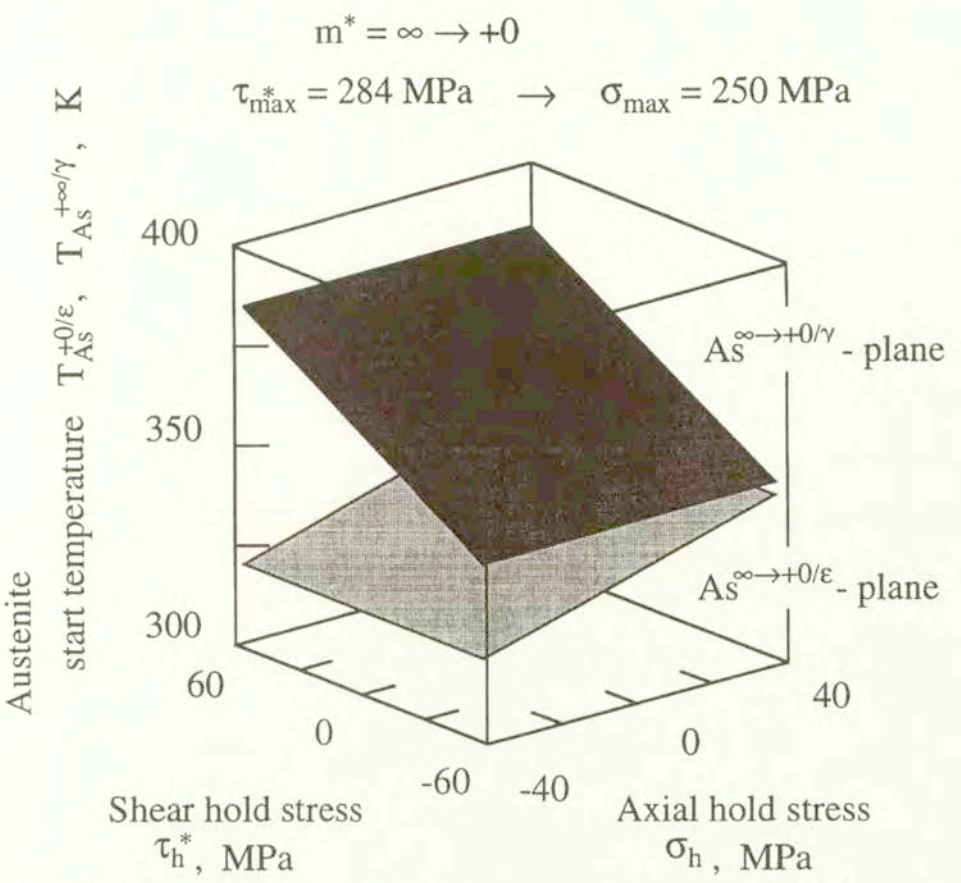

FIG. 19. Austenite start planes after succesive pre-stressing $m^* = \infty$ and $m^* = +0$: $As^{\infty\to+0/\varepsilon}$ -plane is lower in location than $As^{\infty\to+0/\gamma}$ -plane.

The result reveals that the M^{+0} variants first transforms back to the parent phase, and the M^{∞} variants follow later at higher temperature. Under the condition $(\sigma_h, \tau_h^*) = (20\text{ MPa}, -56\text{ MPa})$, however, the reverse is true (cf. Fig. 21).

The result on the austenite start temperatures is summarized in Fig. 22, showing that two austenite start planes now intersect. Compared to the situation in Fig. 19, the $As^{\infty\to+0/\gamma*}$-plane translates to the lower temperature side without changing the slope; in other words, the larger amount of M^{∞} variants formed during shear pre-stressing accelerates the start of reverse transformation during heating. Figure 23, which shows the data projected on the $\tau_h^* - T$ coordinate plane, confirms that the $As^{\infty\to+0/\gamma*}$-plane translates to the lower temperature side, depending on the amount of M^{∞} variants, without changing its slope. A small negative translation of the $As^{\infty\to+0/\varepsilon}$-plane, meaning the retardation of the reverse transformation, which is observed in Figs. 19 and 22, might be due partly to the "isotropic hardening" [9] in the process of shear pre-stressing.

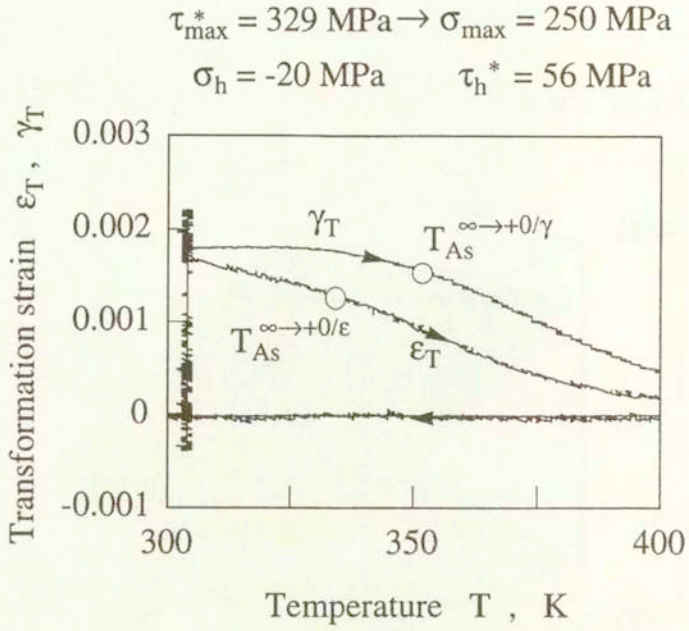

FIG. 20. Recovery of transformation strain during heating: under hold stresses far from inter-section.

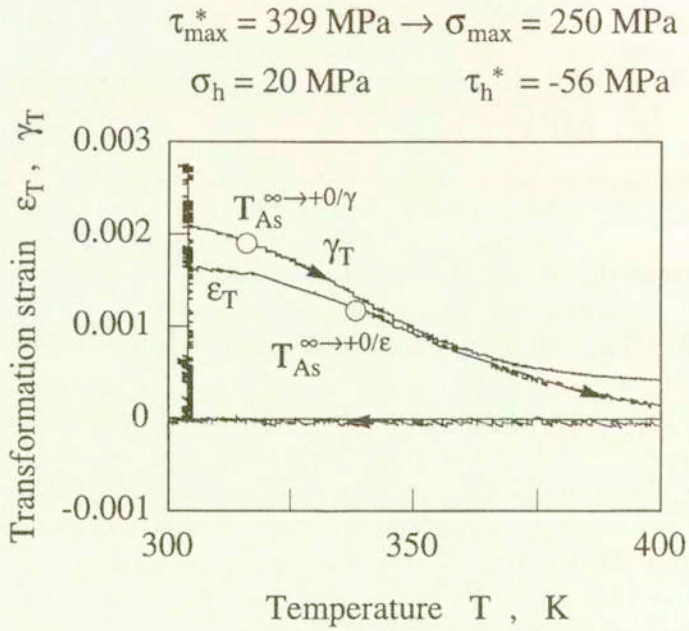

FIG. 21. Transformation strain recovery during heating: under hold stresses near inter--section.

One more important comment in Fig. 22: The reverse transformation starts when the generic point reaches the lower temperature branch of the $As^{\infty\to+0/\varepsilon}$ – and $As^{\infty\to+0/\gamma*}$ -planes. The austenite start condition is, therefore, represented by a bi-plane composed of the branches on the lower temperature side. If, not two martensite variants as discussed here but, many martensite variants are activated in the process of prestressing, the final austenite start condition must be represented by the multi-planes in the stress-temperature space.

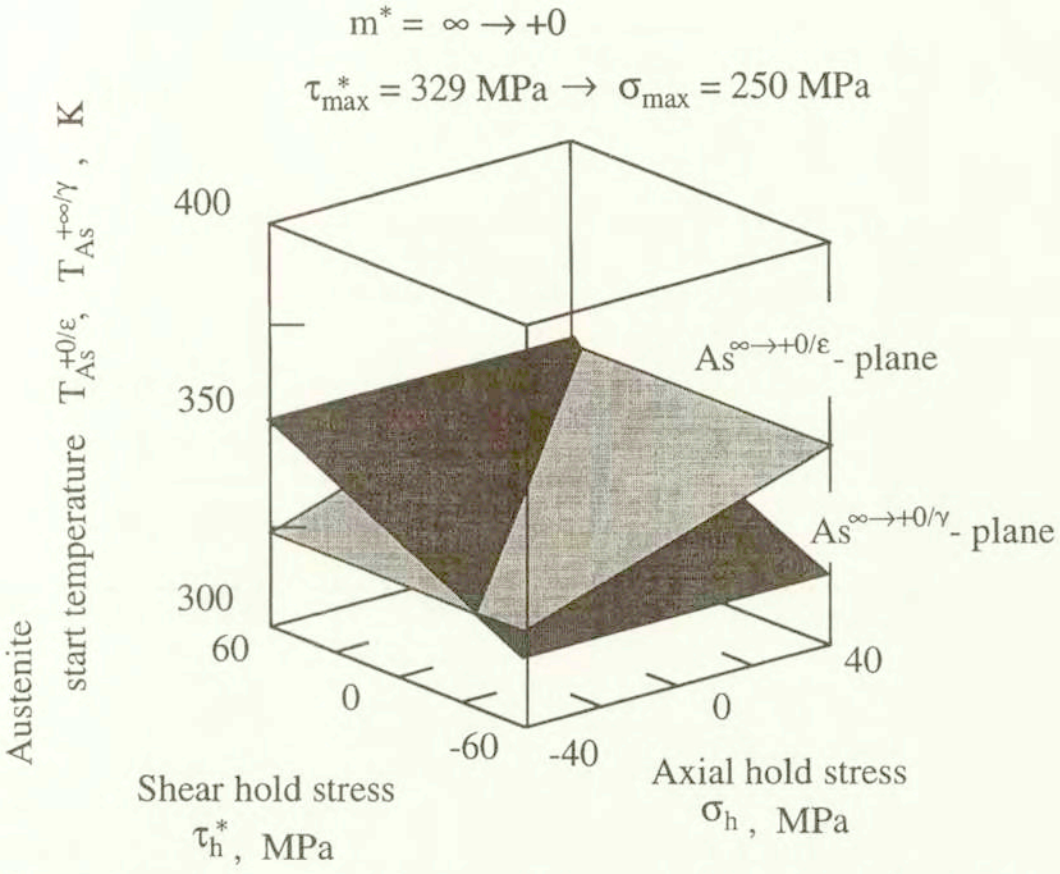

FIG. 22. Austenite start planes after succesive pre-stressing $m^* = -\infty \to m^* = +0$: $As^{\infty\to+0/\gamma}$ -plane translates down, and intersects with $As^{\infty\to+0/\varepsilon}$ -plane.

If the transformation strain intensity $\varepsilon_T^{\text{int}}$ defined in Eq. (2.4) is employed as the parameter to measure the extent of reverse transformation in the multiaxial stress states, the austenite start temperatures $T_{\text{As}}^{\infty\to+0/\text{int}}$ are obtained from $\varepsilon_T^{\text{int}} - T$ dialatation curves. The corresponding austenite start condition is nothing other than the multi-planes explained above, or rather an inscribed surface to the multi-planes. The situation is well explained in Fig. 24. The data points in

the $\sigma_h - \tau_h^* - T$ space are projected, along the intersection of $As^{\infty \to +0/\varepsilon}$ – and $As^{\infty \to +0/\gamma}$ – planes, onto the plane which is perpendicular to both the $\sigma_h - \tau_h^*$ plane and the projection of the intersection onto the $\sigma_h - \tau_h^*$ plane. The data points are actually almost on the lower temperature branches of the $As^{\infty \to +0/\varepsilon}$ – and $As^{\infty \to +0/\gamma *}$ -planes, drawn in a heavy solid line.

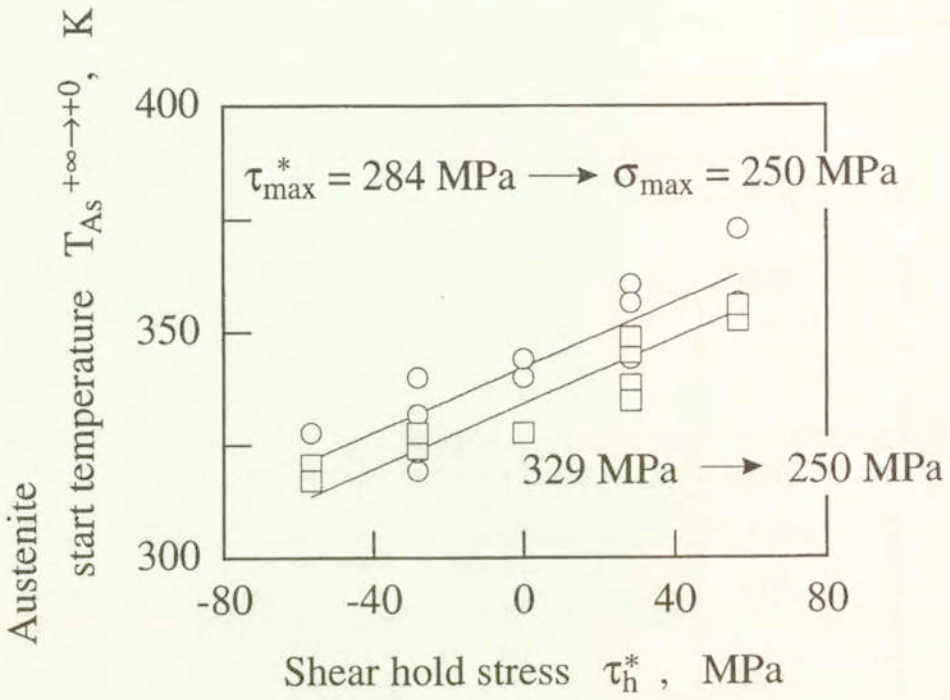

FIG. 23. Translation of austenite start plane.

4.6. Austenite start cone

A cross-section of the transformation start planes in Fig. 22 and an isotemperature plane is shown schematically in Fig. 25(a). The two straight lines, $T_{As}^{+0/\varepsilon}$ -line and $T_{As}^{\infty/\gamma *}$ -line, represent the austenite start lines on the axial hold stress (σ_h) -shear hold stress (τ_h^*) plane, which characterize that start of the reverse transformation of the martensite variants M^{+0} formed during tensile pre-stressing and of the martensite variants $M^{+\infty}$ formed during torsional pre-stressing, respectively. The thick solid line stands for the actual austenite start curve explaining the data.

If the case of compressive pre-stressing is taken into account in addition, Fig. 25(b) would be obtained as the austenite start curve on the $\sigma_h - \tau_h^*$ plane. The curve must be symmetric with respect to the σ_h-axis, but might be asymmetric

with respect to the τ_h^*-axis. If hold stress (σ_h, τ_h^*) is inside the curve, the reverse transformation does not start at this temperature, but, as will be made clear later in Fig. 26, it starts at a higher temperature.

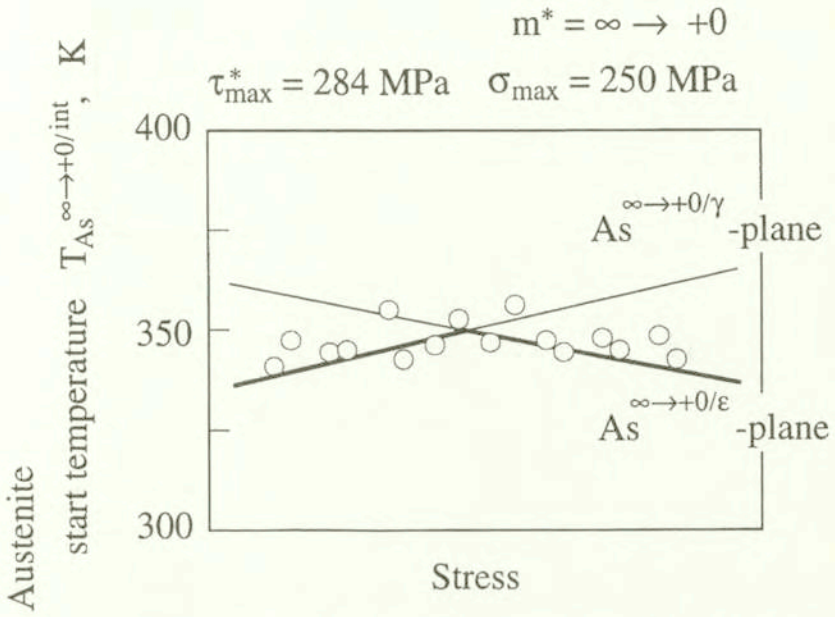

FIG. 24. Austenite start bi-plane constructed from $\varepsilon_T^{int} - T$ dilatation curves.

When the specimen is pre-stressed along a complex non-proportional load path, the austenite start polygon schematically illustrated in Fig. 25(c) would be obtained since many martensite variants with different orientations are activated during pre-stressing.

In the axial hold stress (σ_h) -shear hold stress (τ_h^*) -temperature (T) space, the situation can be sketched schematically by Fig. 26, representing a set of austenite start polygonal cones, the apex of which stands for the austenite start temperature As under stress-free state. The transformation start planes determined experimentally in Fig. 22 are drawn in the figure as the two contact planes.

Summarizing, an austenite start plane is induced in the heating process only when the corresponding martensite variants are formed during preceding martensitic transformation. Each martensite variant characterizes the slope of the plane in the stress-temperature space, whereas the extent of the martensitic transformation determines the position of the plane in the same space. In the case when the martensite variants with some different orientations are formed in the process of mechanical loading, during complex non-proportional loading, for example, the austenite start condition in the stress-temperature space is given by a polygonal cone.

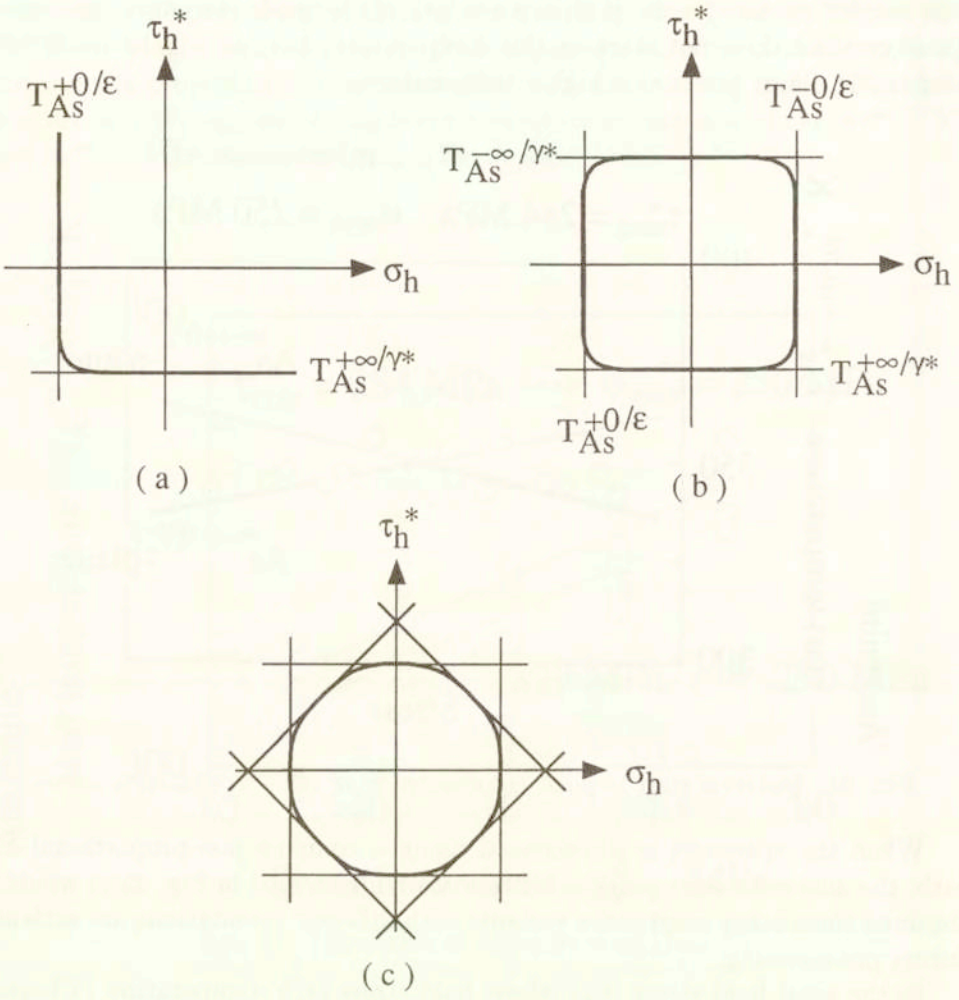

FIG. 25. Austenite start condition on stress plane.

It is worth commenting here on two points: firstly, just at the moment of the start of martensitic transformation, the alloy could exhibit the initial austenite start cone, which correspond to the initial austenite start line determined by the same authors in the uniaxial case [8]. With the progress of the martensitic transformation, the initial austenite cone degenerates into two cones, the austenite start cone and the austenite finish cone, which represent the austenite start and finish conditions, respectively. The latter condition is not discussed in the present study; see Ref. [18] for the case of uniaxial loading, and in Ref. [29] a general outlook of these two austenite start/finish cones are explained.

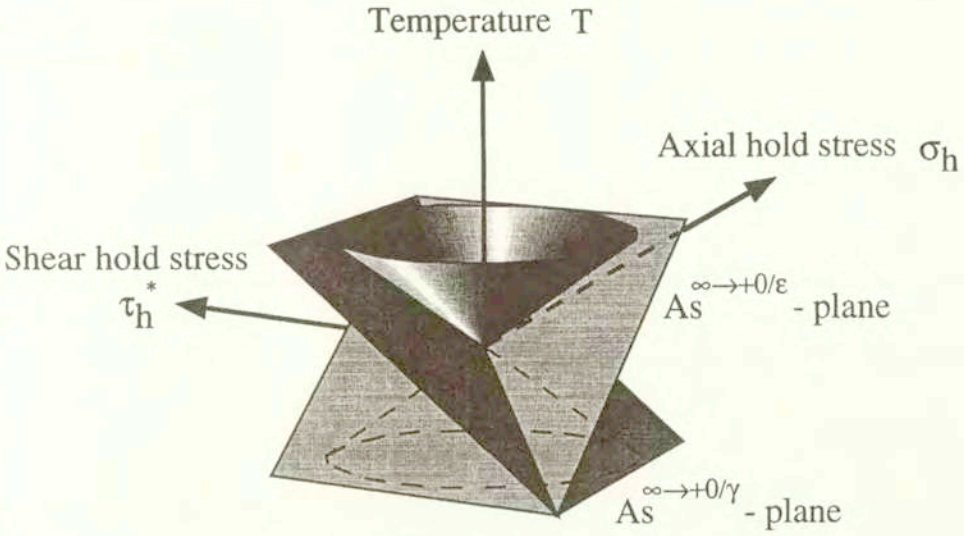

FIG. 26. Austenite start cone in stress-temperature space.

Secondly, one could construct, at each moment of reverse transformation, the subsequent austenite cone between the austenite start and finish cones. The condition is expected to play a role of the plastic potential in the unified theory of transformation/deformation in shape memory alloys [25], just like the subsequent yield condition is the plastic potential in plasticity. Its possibility is determined by checking the normality law associated with the initial martensite start curve. Comprehensive investigations are necessary in this issue.

5. Concluding remarks

The martensite and austenite start conditions are determined experimentally in an Fe-9%Cr-5%Ni-14%Mn-6%Si polycrystalline SMA under combined tension/compression-torsion loads.

The martensite start condition is represented by an oval cone in the stress-temperature space, thus being different from the von Mises theory (the J_2-theory). The asymetry of the start condition with respect to the shear stress axis, a deviation from the J_2-theory, can be well explained by introducing the third invariant of the stress deviator, approving the J_3-theory proposed by RANIECKI *et al.* [10, 12].

The austenite start condition is expressed by a polygonal cone in the same stress-temperature space. Each side of the cone corresponds to the martensite variants preferably induced during mechanical loading. Experiments clearly confirm that the direction of loading determines the direction of the austenite start plane, whereas the amount of variants governs the position of the plane.

Construction of the "subsequent" transformation condition which follows from the initial start condition during thermomechanical loading should be the next urgent topics to be attacked.

Acknowledgments

Part of this work was financially supported by the Special Research Fund/ Tokyo Metropolitan Government as well as by the Grant-in-Aid for Scientific Research (#11650095) through the Ministry of Education, Science and Culture, Japan.

References

1. V. BIRMAN, *Review of mechanics of shape memory alloy structures*, Appl. Mech. Rev., **50**, 629–645, 1997.
2. E.P. GEORGE, R. GOTTHARDT, K. OTSUKA, S. TROLIER-MCKINSTRY and M. WUN-FOGLE [Eds.] *Materials for smart systems* II, Materials Research Society, Pittsburgh 1997.
3. Z.G. WEI, R. SANDSTRÖM and S. MIYAZAKI, *Shape-memory materials and hybrid composites for smart systems, Part* I *and* II, J. Materials Sci., **33**, 3743–3762, 3763–3783, 1998.
4. M. TOKUDA, P. SITTNER, M. TAKAKURA and YE MEN, *Experimental study on performances in* Cu*-based shape memory alloy under multiaxial loading conditions*, Materials Sci. Research Int., **1**, 260–265, 1995.
5. P. SITTNER and M. TOKUDA, *Reorientation in combined stress induced martensite?*, J. Phys. IV, coll. **8**-5, 1003–1008, 1995.
6. P. SITTNER, Y. HARA and M. TOKUDA, *Experimental study on the thermoelatic martensitic transformation in shape memory alloy polycrystal induced by combined external forces*, Metall. Mater. Trans. A, **26A**, 2923–2935, 1995.
7. C. ROGUEDA, C. LEXCELLENT and L. BOCHER, *Experimental study of pseudoelastic behaviour of a* CuZnAl *polycrystalline shape memory alloy under tension-torsion proportional and non-proportional loading tests*, Arch. Mech., **48**, 1025–1045, 1996.
8. F. NISHIMURA, N. WATANABE, T. WATANABE and K. TANAKA, *Transformation conditions in an* Fe*-based shape memory alloy under tensile-torsion loads: Martensite start surface and austenite start/finish planes*, Mater. Sci. Engng. A, **264**, 232–244, 1999.
9. F. NISHIMURA, N. WATANABE and K. TANAKA, *Evolution of martensite start condition in general thermomechanical loads of an* Fe*-based shape memory alloy*, Int. J. Mech. Sci., **42**, 347–365, 1999.
10. B. RANIECKI, S. MIYAZAKI, K. TANAKA, L. DIETRICH and C. LEXCELLENT, *Deformation behaviour of TiNi shape memory alloy undergoing R-phase reorientation in torsion-tension (compression) tests*, Arch. Mech., this issue 1999.
11. K. TANAKA, K. KITAMURA and S. MIYAZAKI, *Shape memory alloy preparation for multiaxial tests and identification of fundamental alloy performance*, Arch. Mech., this issue 1999.
12. B. RANIECKI and CH. LEXCELLENT, *Thermodynamics od isotropic pseudoelasticity in shape memory alloys*, Eur. J. Mech. A/Solids, **17**, 185–205, 1998.

13. E. PATOOR A. EBERHARDT and M. BERVEILLER, *Micromechanical modelling of the shape memory behavior* [In:] L.C. BRINSON and B. MORAN [Eds.], *Mechanics of phase transformations and shape memory alloys*, AMD **189**/PVP **292**, ASME, 23–37, 1994.

14. E. PATOOR and M. BERVEILLER, *Micromechanical modelling of the thermomechanical behavior of shape memory alloys*, [In:] M. BERVEILLER and F.D. FISCHER [Eds.], *Mechanics of solids with phase changes*, 121–188, Springer-Verlag, Wien-New York 1997.

15. K. TANAKA, T. HAYASHI, F. NISHIMURA and H. TOBUSHI, *Hysteretic behavior in an* Fe-Cr-Ni-Mn-Si *polycrystalline shape memory alloy during thermomechanical cyclic loading*, J. Mater. Engng. Performance, **3**, 135–143, 1994.

16. K. TANAKA, F. NISHIMURA and H. TOBUSHI, *Effect of prior transformation on transformation start stress and temperature in an* Fe*-based shape memory alloy*, Z. Metallkde, **86**, 211–215, 1995.

17. K. TANAKA, F. NISHIMURA and H. TOBUSHI, *Transformation conditions and subloops in an* Fe*-based shape memory alloy under thermomechanical loading*, J. Phys. IV, coll.**5**-2, 477–482, 1995.

18. F. NISHIMURA, N. WATANABE and K. TANAKA, *Transformation lines in an* Fe*-based shape memory alloy under tensile and compressive stress states*, Mater. Sci Engng. A, **221**, 134–142, 1996.

19. F. NISHIMURA, N. WATANABE and K. TANAKA, *Hysteretic behavior in an* Fe*-based shape memory alloy under tensile/compressive cyclic thermomechanical loading*, Mater. Sci. Research Int., **3**, 23–30, 1997.

20. F. NISHIMURA, N. WATANABE and K. TANAKA, *Stress-strain-temperature hysteresis and martensitic transformation start line in an* Fe*-based shape memory alloy*, Mater. Sci. Engng. A, **238**, 367–376, 1997.

21. L. ORGEAS and D. FAVIER, *Non-symmetric tension-compression behaviour of NiTi alloy*, J. Phys., coll.8-5, 605–610, 1995.

22. L. ORGEAS and D. FAVIER, *Stress-induced martensitic transformation of a NiTi alloy in isothermal shear, tension and compression*, Acta Mater., **46**, 5579–5591, 1998.

23. T.E. BUCHHEIT, S.L. KUMPF and J.A. WERT, *Modeling the stress-induced transformation behavior of shape memory alloy single crystals*, Acta Metall. Mater., **43**, 4189–4199, 1995.

24. T.E. BUCHHEIT and J.A. WERT, *Modeling the effects of stress state and crystal orientation on the stress-induced transformation of NiTi single crystals*, Metall. Mater. Trans. A, **25A**, 2383–2389, 1994.

25. F.D. FISCHER, E.R. OBERAIGNER, K. TANAKA and F. NISHIMURA, *Transformation induced plasticity revised: an update formulation*, Int. J. Solids Struct., **35** 2209–2227, 1998.

26. S. MIYAZAKI and K. OTSUKA, *Deformation and transition behavior associated with the R-phase in Ti-Ni alloys*, Metall. Trans. A, **17A**, 53–63, 1986.

27. S. MIAZAKI and C.M. WAYMAN, *The r-phase transition and associated shape memory mechanism in TiNi single crystals*, Acta Metall., **36**, 181–192, 1988.

28. S. MIYAZAKI, S. KIMURA and K. OTSUKA, *Shape-memory effect and pseudoelasticity associated with the R-phase transition in Ti-50.5at%Ni single crystals*, Phil. Mag. A, **57**, 467–478, 1988.

29. D.J. BARRETT, *A three-dimensional phase transformation model for shape memory alloys*, J. Intelligent Material Syst. Structures, **6**, 831–839, 1995.

30. F. NISHIMURA, N. WATANABE and K. TANAKA, *Analysis of uniaxial stress-strain-temperature hysteresis in an* Fe*-based shape memory alloy under thermomechanical loading*, Computational Mater. Sci., **8**, 349–362, 1997.

31. K TANAKA, F. NISHIMURA, H. KATO and S. MIYAZAKI, *Transformation thermomechanics of R-phase in TiNi shape memory aloys*, Arch. Mech., **49**, 547–572, 1997.

32. A. BEKKER and L.C. BRINSON, *Temperature-induced phase transformation in a shape memory alloy: Phase diagram based kinetics approach*, J. Mech. Phys. Solids, **45**, 949–988, 1997.

33. A. BEKKER and L.C. BRINSON, *Phase diagram based description of the hysteresis behavior of shape memory alloys*, Acta Mater., **46**, 3649–3665, 1998.

34. K. TANAKA, F. NISHIMURA, T. HAYASHI, H. TOBUSHI and C. LEXCELLENT, *Phenomenological analysis on subloops and cyclic behavior in shape memory alloys under mechanical and/or thermal loads*, Mech. Materials, **19**, 281–292, 1995.

35. H. TOBUSHI, S. YAMADA, T. HACHISUKA, A. IKAI and K. TANAKA, *Thermomechanical properties due to martensitic and R-phase transformations of TiNi shape memory alloy subjected to cyclic loading*, Smart Mater. Struct., **5**, 788–795, 1996.

36. L. FEDERZONI and G. GUÉNIN, *Influence of the presence of pre-existing thermal* ε*-martensite on the formation of stress-induced* ε*-martensite and on the shape memory effect of a* Fe-Mn-Cr-Si-Ni *shape memory alloy*, Scripta Metall. Mater., **31**, 25–30, 1994.

Received March 24, 1999.